

8th U. S. National Combustion Meeting
Organized by the Western States Section of the Combustion Institute
and hosted by the University of Utah
May 19-22, 2013

Optical Investigation of Multiple Injections for Unburned Hydrocarbon Emissions Reduction with Low-Temperature Combustion in a Heavy-Duty Diesel Engine

Jacqueline O'Connor, Mark Musculus
Sandia National Laboratories, Livermore, CA 94566, USA

Low-temperature combustion (LTC) achieved by using exhaust-gas recirculation (EGR) is an operating strategy of current interest for heavy-duty and other compression-ignition (diesel) engines because it offers low nitrogen oxides (NO_x) and soot emissions compared to conventional diesel combustion. While the long ignition-delay of EGR-LTC helps increase pre-combustion mixing to reduce soot formation, other emissions, including unburned hydrocarbons (UHC), can be problematic. Particularly an issue at low-load conditions, a considerable portion of UHC emissions in large-bore diesels are often due to overly-lean fuel/air mixtures formed near the injector during the long ignition delay. In this study, we explore the use of multiple post-injection strategies, which have a large main injection and one or two smaller post injections, to help reduce engine-out UHC emissions. The short post-injections closely timed after the end of the main injection help to enrich the overly-lean region near the injector, allowing for more complete combustion of a greater portion of the fuel/air mixture. Optical results from formaldehyde and OH planar laser-induced fluorescence provide evidence of the in-cylinder spatial and temporal progression toward complete combustion.

1. Introduction

Over the past decade, interest has increased in using low-temperature combustion (LTC) in compression-ignition (diesel) engines as an in-cylinder emissions reduction method [1-4]. LTC operation can significantly reduce NO_x and soot emissions to meet stringent emissions regulation standards while maintaining high fuel-efficiency [5-7].

One way that LTC strategies can achieve low NO_x emissions is through dilution of the intake stream through exhaust-gas recirculation (EGR) [8, 9]. EGR dilution reduces NO_x formation through two mechanisms. First and foremost, the increased concentration of diluents, which include high-heat-capacity species such as CO_2 and H_2O, reduces the flame temperature, and hence slows the chemical kinetics of thermal NO_x formation. In addition, the reactant concentration of oxygen is reduced, which also decreases the NO_x formation rates.

Reduced temperatures at LTC conditions can also decrease soot formation rates, but the lower oxygen concentration simultaneously yields an overall more fuel-rich charge, with can

promote soot formation if pre-combustion mixing is not also modified. LTC strategies enhance pre-combustion mixing by injecting fuel at point in the cycle where the resulting ignition delay is long compared to conventional diesel fuel-injection timings. In this way, the fuel and air are allowed more time to mix, resulting in mixtures that are less fuel-rich at ignition, such that there is much less opportunity for soot formation. This is achieved by injecting fuel either much earlier [10-12] or much later [4, 13] than the conventional diesel fuel-injection schedule. In the case of early injection timings, the fuel is injected into relatively cool, low-density ambient gases. For example, for an early injection starting 20 crank-angle degrees (°CA) before top dead center (TDC) in an engine with a 16:1 compression ratio, when the volume is 55% larger than the TDC volume, the ambient in-cylinder gases are 90-120 K colder and only 70-80% as dense as at 5-10 CA before TDC, when conventional diesel injection usually occurs. Late injections typically start at or slightly after TDC. Even though the ambient gases are hot and dense at the start of the late injection, expansion cooling in the early power stroke and low oxygen concentration from high EGR extends the ignition delay to allow for more premixing prior to combustion. In the present study, we use a late fuel injection timing with favorable combustion phasing for fuel efficiency, starting slightly before TDC, and with 12.6% intake oxygen to achieve LTC.

Changes to the intake charge and injection timing at LTC conditions result in different combustion characteristics and an altered heat release profile from conventional diesel operation. Figure 1 shows a comparison of the commanded injection schedule and apparent heat release rate (AHRR) for typical conventional diesel operation with that of LTC engine operation at low load in our heavy-duty optical diesel engine. The conventional diesel operating condition uses some dilution (18% intake oxygen), which is typical of modern production diesel engines, while the LTC condition uses much more dilution (12.6% intake oxygen) than in typical modern production diesel engines. Details of the injection schedule, including the commanded start of injection ($SOI1_C$) and commanded injection duration ($DOI1_C$) are provided in the caption.

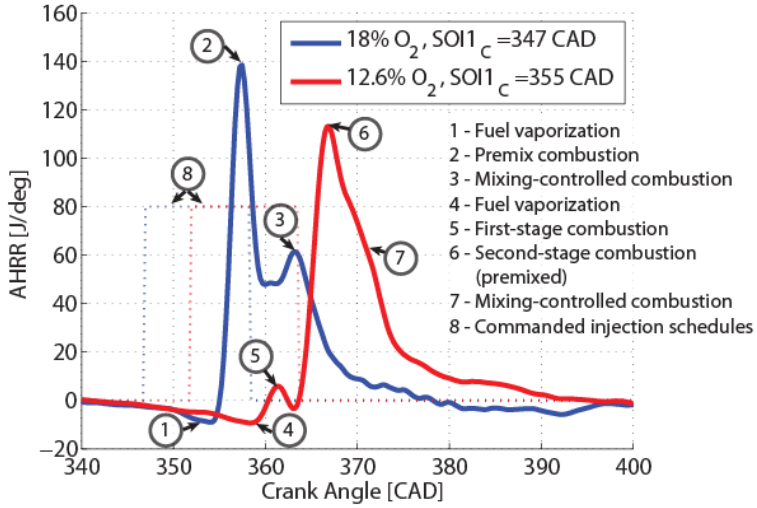

Figure 1. Comparison of commanded injection schedule (dotted lines) and apparent heat release rate (solid lines) for conventional diesel combustion at 18% intake O_2 and $SOI1_C$=347 CAD, $DOI1_C$=1550 microseconds (blue) with LTC combustion at 12.6% O_2 and $SOI1_C$=355 CAD, $DOI1_C$=1600 microseconds (red). Important features of the AHRR and the injection schedule are annotated.

Important differentiating features of the AHRR profile for conventional diesel and LTC profile are numbered in Figure 1. For both types of combustion, the actual start of fuel injection, when fuel begins to emerge from the nozzle, occurs about 3 °CA after the start of the command pulse (i.e., after $SOI1_C$). Notice in the traditional diesel profile that after fuel injection near 350 CAD, the heat release dips due to fuel vaporization (1), followed by two combustion events: the premixed burn (2) and the mixing-controlled combustion (3). The premixed burn happens as a result of some fuel/air premixing that occurs during the ignition delay between the start of injection and autoignition. For this low-load condition, the mixing-controlled combustion has a lower peak AHRR, but it lasts much later into the cycle as the remaining fuel and air mix and react. While the two peaks in the AHRR can be generally attributed to premixed burning and mixing-controlled combustion, they are not entirely separate, and some elements of both can occur throughout the conventional diesel combustion event. A more detailed description of conventional diesel combustion may be found elsewhere (e.g., [14, 15]), and will not be discussed further here.

During LTC combustion, fuel vaporization (4) is also apparent, but thereafter, the AHRR profile differs from the conventional diesel profile. First, a low-temperature chemistry event, often termed a "cool flame," occurs after the first-stage ignition, resulting in a small bump in the AHRR (5). The same first-stage combustion also occurs during conventional diesel combustion, but because of the lower dilution levels and shorter ignition delay, it is more rapid and less prominent, so it is not usually apparent as a distinct event in the AHRR profile. After a short dwell following the first-stage combustion, second-stage ignition is characterized by a larger spike, with a much higher peak AHRR (6). The second-stage ignition event is followed by a mixing-controlled burn (7) that is less pronounced than for conventional diesel combustion. The majority of the heat release during LTC operation typically arises from partially-premixed combustion as a result of the long ignition delay. In the LTC case shown in Figure 1, the ignition delay from the start of injection to the start of main (second-stage) combustion is approximately 9.1 °CA (1270 microseconds), compared to only 7 °CA (973 microseconds) for the conventional diesel condition. The longer ignition delay allows more time for the fuel to mix with ambient gases prior to the second-stage ignition. Even with an extended ignition delay, for this particular LTC condition, some of the fuel must mix after combustion is initiated, so that some mixing-controlled combustion occurs after the second-stage ignition. Nevertheless, the prominence of both first-and second-stage combustion events for this LTC condition indicates that combustion chemistry has changed significantly with low intake-oxygen levels and a long ignition delay.

While the enhanced mixing and charge dilution that characterize LTC combustion can work to suppress NO_x and soot emissions, they typically exacerbate the levels of other emissions, including carbon monoxide and unburned hydrocarbons (UHC). While many sources of UHC have been identified in the literature for both light-duty and heavy-duty engines [1, 16, 17], the focus of this study is characterization and reduction of lean-source UHC in heavy-duty diesel engines at low-load conditions. When the ignition delay is long, a lean fuel/air mixture in the center of the bowl (near the injector) is formed after the end of fuel injection [18]. It has been proposed that enhanced entrainment during the fuel-jet ramp down at the end of injection creates the lean fuel/air mixture in the center of the bowl [19]. The mixture in this region, having advanced through first-stage combustion, is too lean and too cold to proceed to second-stage combustion. As a result, a portion of the reactants never complete combustion, resulting in significant UHC and CO emissions.

A proposed solution for reducing this source of UHC is the use of multiple injections [20-22]. If properly executed, a short, close-coupled post injection can enrich the overly-lean region close to the injector, potentially "kicking" it into second-stage combustion and completing combustion of a larger portion of the in-cylinder hydrocarbons. A previous study in our engine by Chartier *et al.* [20] showed that close-coupled post injections have potential for UHC emissions reduction. Figure 2 shows a summary of their results that are relevant to this study. The plot on the left shows three injection-rate shapes: one using a single injection and two using a main injection with either a small or a large post injection. The plot on the right shows the trend of increasing UHC emissions as load decreases for single-injection operation. The two post-injection conditions studied in [20] either fall directly on top of the single-injection trend line (large post injection) or result in an approximately 20% reduction in UHC compared to a single injection at the same load (small post injection).

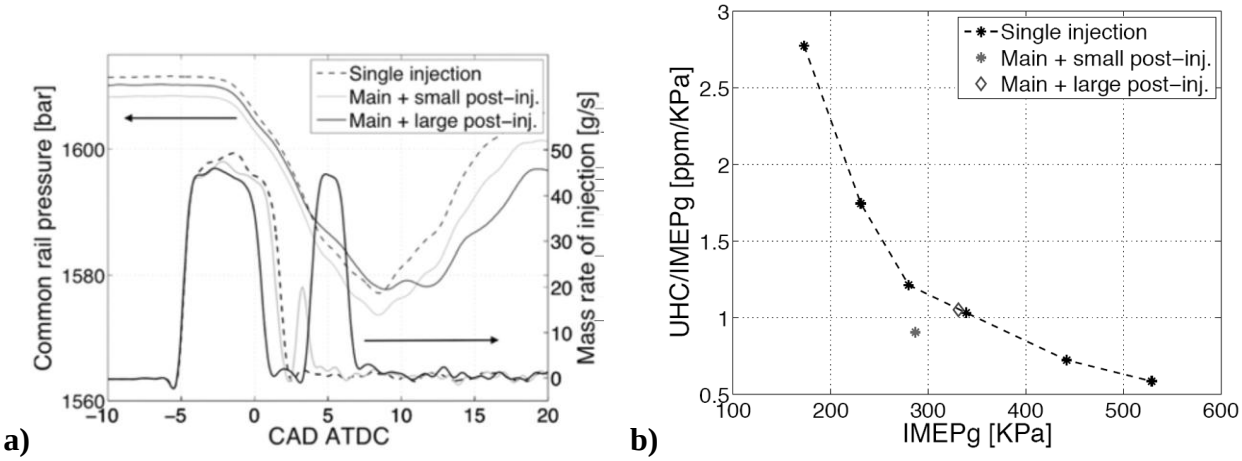

Figure 2. Injection rate profile (a) and engine-out UHC levels versus load (b) for three operating LTC conditions: single injection, main plus small post injection, and main plus large post injection [20].

These results clearly indicate that a short, close-coupled post injection can reduce engine-out UHC levels at certain conditions. Additional optical data in [20] show that the in-cylinder progression of combustion is consistent with enrichment of the overly-lean fuel/air mixture near the nozzle, which promotes second-stage combustion to a greater extent.

While post-injections have shown promise for UHC reduction, implementation of a multiple-injection strategy introduces many new variables to the parameter space, making the design of an effective injection schedule difficult. Additionally, there is still much to understand about the mechanism by which UHC emissions are reduced using multiple injections; further optical investigation is required to better describe these processes. In this study, we investigate the mechanisms of UHC emissions reduction by main- plus post-injection schedules with either one or two close-coupled post injections (i.e., a total of either two or three injection events per cycle). These results are compared to a single-injection baseline to quantify the improvements available with these two types of injection schedules. While the parameter space is far too vast to explore completely in a study such as this, the data provide us with a baseline by which to further investigate the role of multiple injections in UHC emissions reduction.

The remainder of this paper is organized as follows. The first section is an overview of the experimental setup, including details of the optical engine experiment, engine operating conditions, test matrix, and optical diagnostics. Next, the results of the three injection schedules

are discussed. Here, results from both engine-out UHC measurements and in-cylinder laser-induced fluorescence imaging of combustion intermediate species are used to understand the effect that multiple injections have on UHC emissions and their formation. Finally, we provide several conclusions from this study with a discussion of design-level concerns regarding implementation of multiple-injection schedules for UHC reduction at LTC conditions.

2. Experimental setup

2.1 Optical Engine Experiment

The optical engine is based on a single-cylinder version of the Cummins N-series direct-injection, heavy-duty diesel engine. The engine has a bore of 139.7 mm and a stroke of 152.4 mm, and is equipped with a Bowditch piston with an open, right-cylindrical bowl and a flat piston-crown window providing imaging access to the bowl, from below. A flat, round window is also installed in place of one of the exhaust valves for imaging access to a portion of the squish region above the piston (view not used in the current study). A 30-mm wide curved window matching the contour of a portion of the bowl-wall allows laser access into the bowl. Additional laser access is available through flat rectangular windows installed in a ring at the top of the cylinder. Information about engine geometry is in Table 1 and a schematic of the experiment is in Figure 3. Further details about this engine can be found in Refs. [15, 23].

Table 1. Engine and fuel system specifications.

Engine base type	Cummins N-14, DI diesel
Number of cylinders	1
Cycle	4-stroke
Combustion chamber	Quiescent, direct injection
Swirl ratio	0.5 (approx.)
Bore	139.7 mm [5.5 in]
Stroke	152.4 mm [6.0 in]
Bowl width	97.8 mm [3.85 in]
Displacement	2.34 liters [142 in^3]
Geometric compression ratio	11.2:1
Replicated compression ratio	16:1
Fuel Injector	Delphi DFI-1.5 (light duty)
Fuel injector type	Common-rail, solenoid actuated
Number of holes & arrangement	8, equally-spaced
Spray pattern included angle	156°
Nominal orifice diameter	0.131 mm

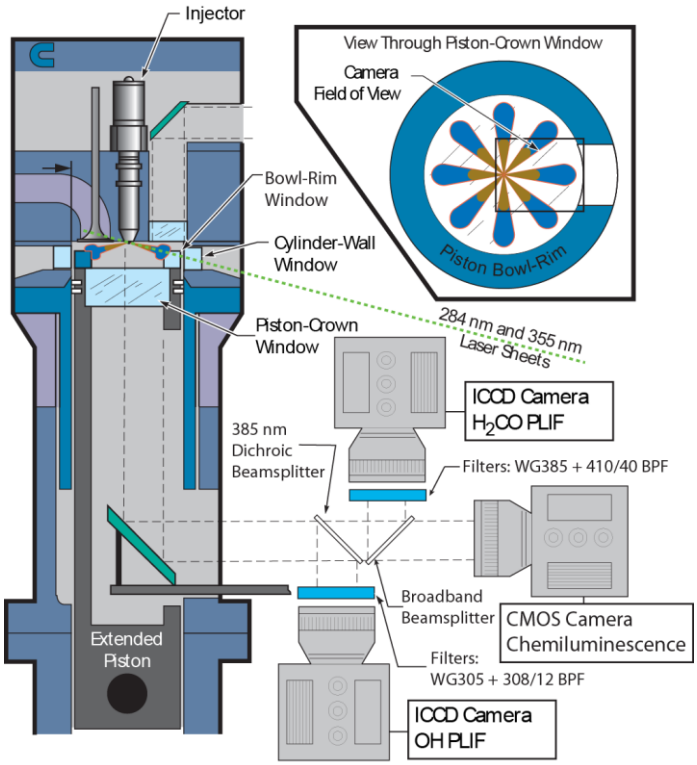

Figure 3. Experimental setup of the single-cylinder optical engine, laser configuration, and three-camera optical system. The camera field-of-view is shown in the upper right.

A Delphi DFI 1.5 light-duty, solenoid-driven common-rail injector with eight equally spaced 131-micron orifices with an included angle of 156° is centrally located on the cylinder axis. This light-duty injector was used in place of the previous heavy-duty injector for its fast response time and its ability to deliver consistent, close-coupled, short-duration post injections over a range of low-load injection schedules. Because of the low lubricity and low viscosity of special fuels (such as n-heptane) selected for optical research, the production common-rail fuel pump could not be utilized. Instead, a custom high-pressure diaphragm pump specially designed for low-lubricity fuels pressurizes the fuel rail at up to 2000 bar. The delivery rate of the diaphragm pump is limited, however, and as a result it could only sustainably pressurize the fuel rail to 1200 bar at the static back-leak rate of this particular injector.

2.2 Engine Operating Conditions

The engine is operated in a late-injection LTC mode, for which the start of main combustion begins slightly after TDC, near the peak-efficiency phasing. As discussed above, UHC emissions are a particular issue at low-load conditions; the engine load range in this study is varied between one (1) and approximately six (6) bar gross, indicated mean-effective-pressure (gIMEP). More details about the engine operating conditions are in Table 2.

.

Table 2. Engine operating conditions.

Engine Speed	1200 RPM
Engine Load Range	100-600 kPa gIMEP†
Intake O_2	12.6%
Fuel Pressure	1200 bar
TDC Motored Density	18 kg/m^3
TDC Motored Temperature	837 K
BDC Pressure	164 kPa
BDC Temperature	78 °C
(16:1 Compression Ratio BDC Pressure)	101 kPa (abs)
(16:1 Compression Ratio BDC Temperature)	36°C

†gIMEP is the calculated work done during compression and expansion strokes only, using the measured cylinder pressure.

As described earlier in the discussed of Figure 1, the AHRR for this partially-premixed combustion mode displays a small first-stage (cool-flame) ignition peak followed by a large second-stage peak and a small mixing-controlled combustion tail. The addition of a post injection typically adds another small peak to the heat release curve after the main second-stage ignition. These features are illustrated in Figure 4.

In this paper, we will use the following terminology to refer ignition and combustion events. Ignition refers to the start of each event; from the AHRR curve in Figure 4, first-stage *ignition* happens at approximately 360 CAD and second-stage *ignition* near 363 CAD. First- and second-stage *combustion* are the ensuing reactions that are sustained after ignition. This terminology will be utilized, and further distinctions will be provided, when discussing the optical data in Section 3.

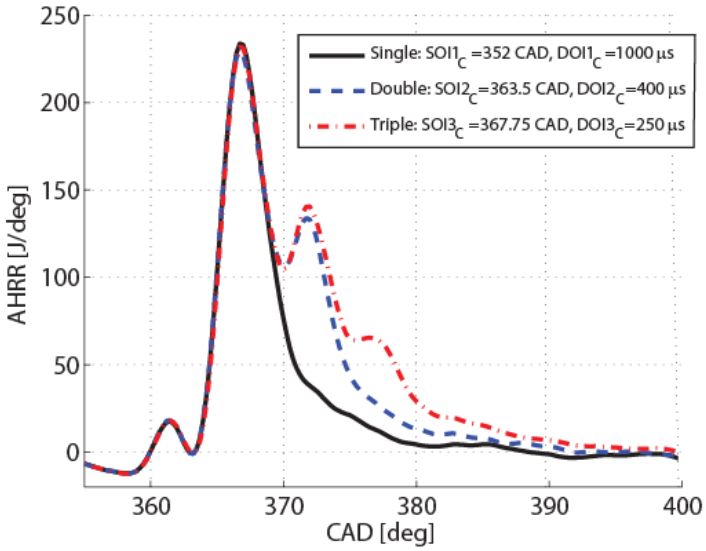

Figure 4. Apparent heat release rate for single injection (black solid line) with $SOI1_C$ =352 CAD and $DOI1_C$ =1000 microseconds, a main plus one post injection (blue dotted line) with $SOI2_C$ =363.5 CAD and $DOI2_C$ =400 microseconds, and a main plus two post injections (red dot-dash line) with $SOI3_C$=367.75 CAD and $DOI3_C$=250 microseconds.

The ignition delays of the first and second post injections are 3.8 °CA and 3.2 °CA, respectively, much shorter than the 9.1 °CA ignition delay of the main injection. This is to be expected as the ambient pressure and temperature are much higher during the post and third injections as a result of combustion from earlier-injected fuel. Even so, the injection duration is short, such that ignition for both the post and the third injections occurs after the end of each fuel injection event. Consequently, some premixing occurs prior to ignition of the post-injection fuel.

2.3 Test Matrix

The test matrix in Table 3 outlines the three types of tests to measure the effect of multiple injections on engine-out UHC reductions. While UHC emissions were measured at each of these points, PLIF images are available at a smaller subset of these conditions.

Table 3. Engine operating test matrix with commanded injection timings and durations.

% O_2	$SOI1_C$ [CAD]	$DOI1_C$ [microsec.]	$SOI2_C$ [CAD]	$DOI2_C$ [microsec.]	$SOI3_C$ [CAD]	$DOI3_C$ [microsec.]
12.6	352	600-2400				
12.6	352	1000	363.5	200-800		
12.6	352	1000	363.5	300	367.75	250
12.6	352	1000	363.5	450	370	250

The test matrix contains three types of injection schedules: single-injection schedules, main- plus one post-injection schedules, and main- plus two post-injection schedules. To establish consistent terminology, an injection schedules with only one injection is called a "single-injection." An injection schedule with two injections, a main injection and a post injection, is termed a "main- plus one post-injection." Here, a "main injection" is by definition longer than a post injection. Finally, an injection schedule with three injections, a main injection plus two post injections, is termed "main- plus two post-injections." Here again, the main injection is a long injection that is followed by two shorter post injections. In these particular tests, the second post injection is smaller than the first one, the rationale for which is described below in the results.

2.4 Engine Diagnostics

Several diagnostics are used to investigate the origin of UHC emissions at LTC conditions. Cylinder pressure is measured with an AVL QC34D pressure transducer every quarter crank-angle degree. The AHRR (Figure 4) is calculated from the measured cylinder pressure using standard techniques described in Ref. [14].

Engine-out UHC emissions are measured with a California Analytical Instruments (CAI) 600-series hydrocarbon analyzer. This analyzer samples the exhaust stream and uses a flame ionization detector to measure total unburned hydrocarbons, reported as ppm C_1 (i.e., methane). The exhaust stream is pulled from the exhaust manifold, within 100 mm of the exhaust valve. The 3-m line from the engine to the analyzer is heated to 155 degrees Celsius to minimize condensation of water and hydrocarbons. A pump provides a continuous flow of exhaust gases to the analyzer, and the transit time between the engine and the analyzer is about 4 seconds. All UHC data are averaged over a run time of 100 fired cycles. To account for the skip-fired operation of the engine, the reported UHC results have been multiplied by 10 to approximate

what they would be in a continuously-fired, single-cylinder engine. The standard deviation of UHC measurements for repeated runs is approximately 2 ppm (corresponding to 20 ppm after correcting for a continuously-fired engine).

Three different optical diagnostic techniques are employed to gain insight into the origins of UHC emissions. Although in-cylinder UHC is not measured directly, two important radical species involved in ignition provide information about the evolution of in-cylinder unburned fuel. Formaldehyde (H_2CO) is produced during first-stage ignition, is present throughout first-stage combustion, and is consumed during second-stage ignition. Detailed chemical kinetics simulations predict that after first-stage ignition, the evolution of formaldehyde mirrors that of the overall pool of unburned hydrocarbons [24]. Hence, formaldehyde serves as a marker of unburned fuel from mixtures that have achieved first-stage ignition but have not yet reached second-stage ignition. Formaldehyde does not serve as a good marker for unburned fuel in regions that have not achieved first-stage ignition (e.g., from wall wetting and potentially crevices), nor does it mark UHC in rich mixtures after second-stage ignition. However, previous studies [18, 24] have shown that in the near injector region, overly-lean mixtures are a primary source of UHC emissions, so that formaldehyde serves as a good marker for those UHC sources.

The second radical species, the hydroxyl radical (OH), rises in concentration by orders of magnitude at second-stage ignition in fuel-lean to stoichiometric mixtures [25], and remains thereafter throughout second-stage combustion. The OH distribution provides an indication of second-stage ignition and relatively complete combustion, and hence relatively complete oxidation of unburned hydrocarbon species.

As described below, two laser-based techniques are used to measure these two radical species, similar to previous studies conducted at LTC conditions in this engine [20, 24]. Both laser-based techniques used 10 Hz repetition-rate lasers, allowing one image to be taken per cycle.

Planar laser-induced fluorescence of formaldehyde (H_2CO-PLIF): The third harmonic output of a Spectra-Physics Quanta-Ray single-cavity Nd:YAG laser at a wavelength of 355 nm is formed into a 30-mm wide, approximately 1-mm thick sheet with 80 mJ per pulse at the engine for laser-induced fluorescence of formaldehyde within the engine cylinder. The sheet is oriented at a 12° angle relative to the firedeck to probe H_2CO along the approximate symmetry plane of one of the fuel sprays. LIF emission is collected with an intensified Princeton Instruments PI-MAX 3 intensified charge-coupled device (ICCD) camera with a HQf (GEN-III) intensifier and a resolution of 1024x1024, a gate time of 50 ns, and at maximum gain. A Nikkor glass f/2.5 lens is used. Two filters, a 385 nm long-wave-pass and a 40-nm wide bandpass filter centered at 408 nm, reject laser scatter and other interference outside the formaldehyde fluorescence emission band.

Planar laser-induced fluorescence of OH (OH-PLIF): A Spectra-Physics Quanta-Ray single-cavity Nd:YAG laser is used in conjunction with a Spectra-Physics optical parametric oscillator (OPO) to produce the laser excitation for the OH-PLIF technique. The OPO is tuned to near 568 nm and the light is doubled using a BBO crystal to approximately 284 nm to excite the Q1(9), Q2(8), and P1(5) transitions of OH that merge as a result of pressure broadening. The 284-nm laser beam is co-aligned with the 355-nm laser beam for H_2CO-PLIF upstream of any sheet optics. As a result, the laser sheet at 284 nm is approximately the same size as that at 355 nm: 30-mm wide and 1 mm thick. The 284-nm laser pulse energy at the engine is 19 mJ. LIF emission is collected with an intensified Princeton Instruments PI-MAX 3 ICCD camera with a

super-blue, slow-gate intensifier (Gen-II) and a resolution of 1024x1024, a gate time of 410 ns, and at maximum gain. An ultraviolet (UV) Nikkor f/4.5 lens is used. Three filters, a 65-nm wide blocked bandpass filter at 310 nm, a 15-nm wide unblocked bandpass filter at 310 nm, and a color-glass SWG305, reject laser scatter and other interference outside the OH fluorescence band near 308 nm. Detuning the laser off the transition at 284 nm produces almost no signal though the filter pack, indicating that the signal shown in the OH-PLIF images is almost entirely fluorescence of OH.

For both laser-induced fluorescence techniques, the LIF data are limited to one frame per cycle, due to repetition-rate constraints of both the laser and camera system. The OH-LIF signal is collected 1 microsecond before that of the H_2CO-LIF signal, so that they are virtually simultaneous relative to engine time scales. As shown in Figure 3, the fluorescence emission is collected through the large piston-crown window and directed to the two ICCD cameras and to one high-speed complementary metal oxide semiconductor (CMOS) camera using two beamsplitters. A long-wave-pass beamsplitter with a cut-off near 385 nm directs UV light to the OH-PLIF camera. The remaining light is split by a 50% reflectance broadband beamsplitter between the H_2CO-PLIF camera and the high-speed CMOS camera for natural luminescence imaging (described below).

These two LIF techniques are used together to simultaneously image intermediate species after first- and second-stage ignition. As described above, H_2CO is a marker of UHC remaining after first-stage ignition, while OH is a marker of second-stage ignition [24] and concomitant consumption of UHC. It has been shown in previous studies as well as the current work that these two signals generally do not overlap within the plane of the lasers, and that the location where they meet is an indication of the transition from first- to second-stage combustion. An example of this is Figure 5, which is annotated to show each region. The figure shows a partial view of the piston bowl from below, with the injector on the left (white dot) and the wall of the right-cylindrical bowl on the right (as indicated by a curved white line). The format of this figure will be used throughout this manuscript to show the H_2CO-PLIF and OH-PLIF images.

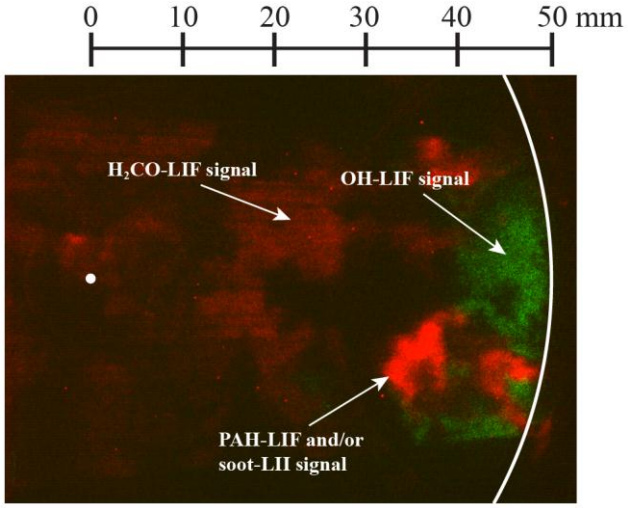

Figure 5. Example of simultaneous H_2CO-PLIF (false-colored red) and OH-PLIF (green) imaging at 373 CAD for an LTC, single-injection case at 12.6% intake O_2, $SOI1_C$=352 CAD, $DOI1_C$=800 microseconds. The injector and bowl rim locations are indicated by the white dot and curved line, respectively.

In Figure 5, the two false-colors indicate the two species under consideration: red for H_2CO and green for OH fluorescence. It is clear that they overlap very little within the plane of the laser, which is consistent with of the use of these two species as markers for the first- and second-stage ignition regions. Later in the cycle, generally after OH fluorescence is first detected, the 355 nm laser can excite not only H_2CO molecules, but also poly-cyclic aromatic hydrocarbon (PAH) molecules, which are precursors to soot, as well as possible laser-induced incandescence (LII) of soot itself. The emission spectrum and signal intensity of fluorescence from these laser-excited PAH molecules are different from H_2CO, and hence can be used to discriminate between the two sources.

Our previous studies of LTC conditions using simultaneous OH- and H_2CO-PLIF imaging used a spectrometer to discriminate between H_2CO and PAH fluorescence and/or soot LII [20]. The H_2CO fluorescence spectrum shows a series of characteristic bands within the filter bandpass, while both PAH fluorescence and soot LII spectra are relatively broadband. Additionally, inspection of the images showed that the intensity of the broadband PAH/soot emission was almost universally much brighter and more isolated than the H_2CO emission, which remained relatively unchanged until its disappearance at second-stage ignition. The close correlation between the spectral signatures and intensity patterns of H_2CO and PAH/soot allow discrimination by intensity, without using a spectrometer. For instance, the broad, relatively moderate intensity fluorescence from 355-nm excitation on the left half of Figure 5 (dark red color) is characteristic of formaldehyde fluorescence, while the more isolated, intense pockets of emission on the right side of the image (bright red color) are typical of PAH fluorescence and/or soot LII, as labeled in Figure 5. To allow simultaneous use of with all three imaging diagnostics, and due to our confidence in interpretation of the H_2CO-PLIF images according to intensity, we did not use a spectrometer to discriminate between formaldehyde and PAH fluorescence.

High-speed natural luminescence imaging: The third technique uses a Phantom 7.1 CMOS camera equipped with a Nikkor 105 mm, f/1.8 lens to record natural luminescence from combustion reactions and combustion-generated products. The camera framing is triggered by the shaft encoder at a resolution of one-half ºCA, and the exposure duration is 50 microseconds. Although first-stage ignition reactions yield some weak chemiluminescence that sometimes can be detected with CMOS arrays, in the current study the intensity is too weak after the two beam-splitters for the laser diagnostics. Hence, any ignition chemiluminescence visible in the high-speed images is from second-stage ignition. Natural soot luminescence, when present, is also recorded by the camera. The high-speed natural luminosity images are not presented in the present study, but some information gleaned from inspection of the images (e.g., spray/jet penetration and actual injection start/dwell times), is discussed.

3. Results

The results are presented in three sections, each addressing the engine-out UHC emissions measurements and accompanying OH-PLIF and H_2CO-PLIF measurements at the three different types of injection schedules. Overall, the results show that multiple injections reduce engine-out UHC, consistent with enrichment of the overly-lean mixture near the injector. The addition of one post injection reduces the UHC emissions from the single-injection levels, and a main- plus two post-injection schedule reduces the UHC emissions even further from the main- plus one post-injection levels. In both cases, the additional injection helps to “kick” the first-stage

combustion into second-stage ignition near the injector, as evidenced by the greater extent of OH-PLIF signal throughout the combustion chamber, especially in the near-injector regions that would have been occupied by H_2CO-PLIF.

3.1 Single-injection baseline

Single-injection tests establish a baseline UHC emissions curve against which to judge the performance of the multiple-injection schedules. Figure 6 shows the engine-out UHC measurements over a range of commanded injection durations, from 600 microseconds to 2400 microseconds at $SOI1_C$=352 CAD.

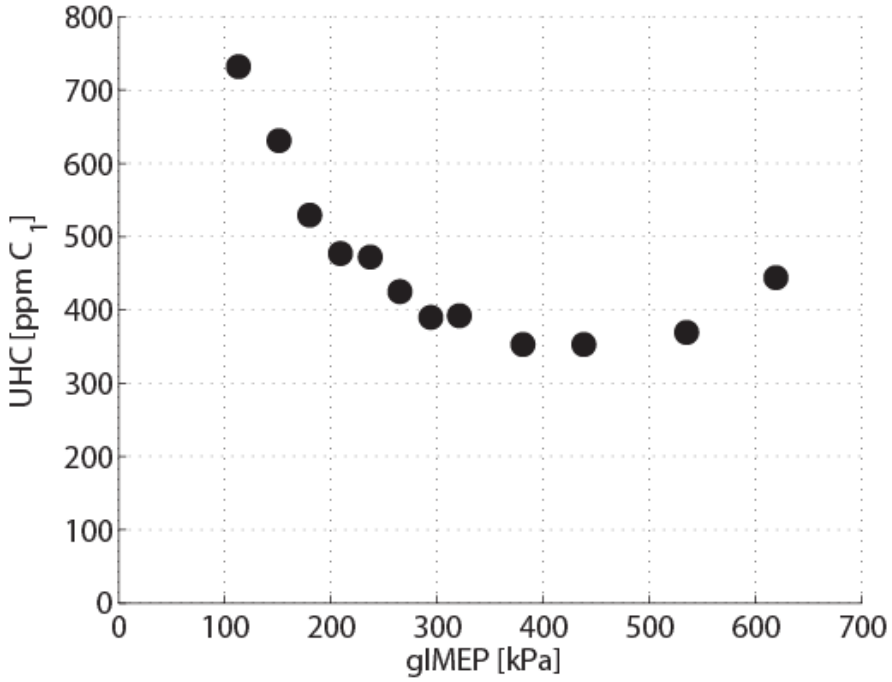

Figure 6. Engine-out UHC emissions for single-injection operation ($SOI1_C$=352 CAD) at a range of $DOI1_C$ from 600 to 2400 microseconds. UHC emissions have been corrected from skip-fired operation to reflect those of continuous-fired operation.

The high levels of UHC for the very short injection-duration cases (100-150 kPa gIMEP with $DOI1_C$ = 600-700 microseconds) stem from the fact that there were partial burns at very low loads. At the mid-range injection durations (200-500 kPa gIMEP with $DOI2_C$ = 800-2000 microseconds), the bulk of the UHC emissions stems from the overly-lean region near the injector, as discussed in the Introduction. A minimum UHC level is observed near 400 kPa gIMEP ($DOI1_C$=1400 microseconds). At longer injection-duration conditions (gIMEP > 500 kPa, $DOI1_C$ = 2000-2400 microseconds), UHC emissions likely stem from both lean and rich sources. That is, while some UHC emissions still originate from the overly-lean region in the center of the bowl, incomplete combustion in rich regions likely begin to contribute to UHC due to the increased injection duration and late phasing of the latter part of the fuel injection.

Figure 6 is important as a baseline reference because it shows how UHC emissions are affected by load for single-injection conditions. When evaluating any effects on UHC emissions by post injections, the change in load due to the fuel added by the post injection must be

considered. As will be shown in the next two sections, Figure 6 allows the post-injection effects on UHC to be quantitatively evaluated relative to single-injection operation with proper consideration of load effects.

A series of instantaneous images showing the spatial and temporal progression of the single-injection combustion process are in Figure 7. Here, H_2CO-PLIF signal (red) provides an indication of the regions undergoing first-stage combustion, whereas the OH-PLIF signal (green) indicates where second-stage combustion is taking place.

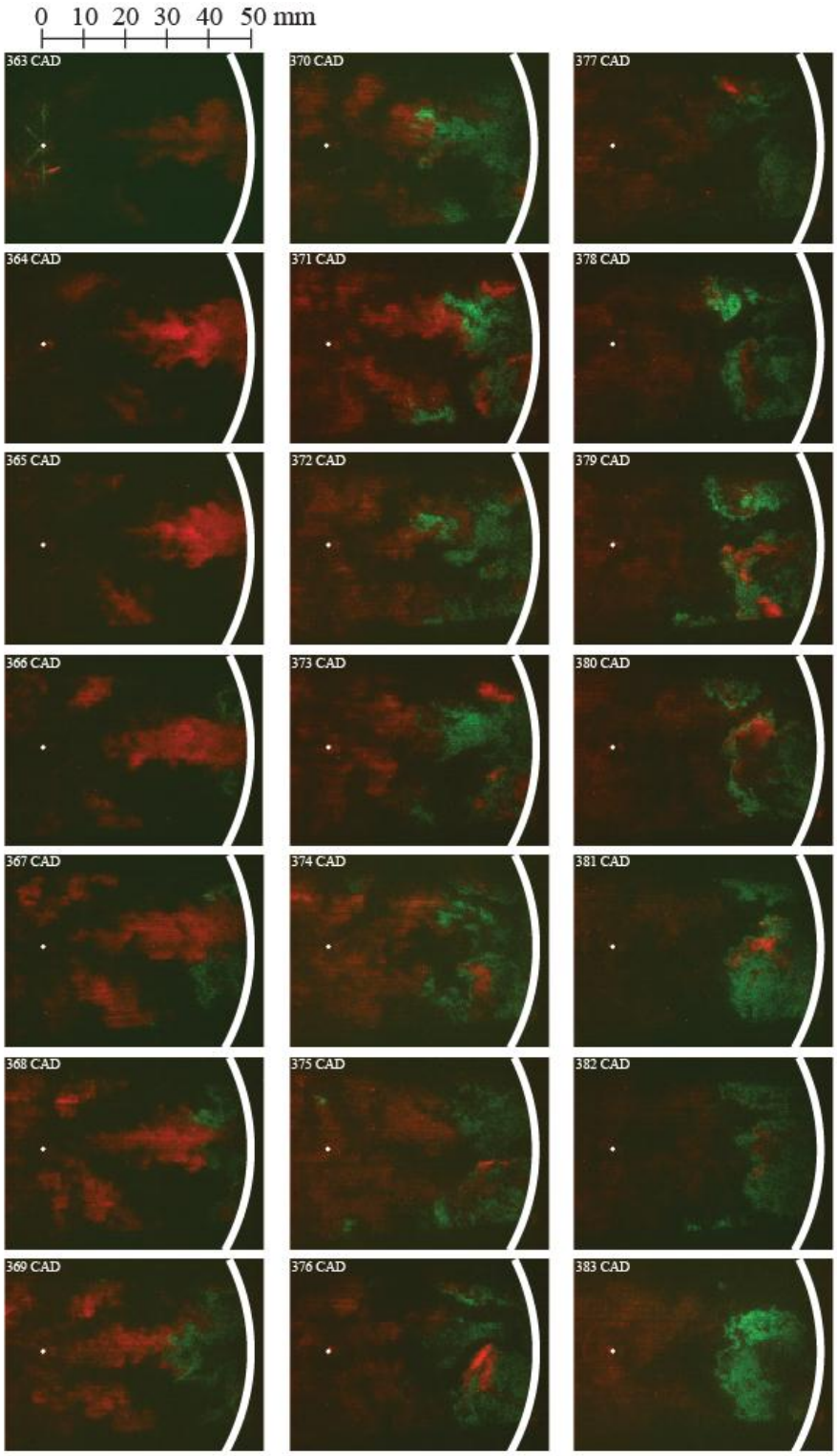

Figure 7. Single-shot simultaneous H_2CO-PLIF (false-colored red) and OH-PLIF (green) images for a single-injection case at $SOI1_C$=352 CAD, $DOI1_C$=1000 microseconds, and 256 kPa gIMEP.

The series in Figure 7 begins at 363 CAD, which is near the end of injection. Here, a weak signal from Mie scattering of the 284 nm laser (shown in green) off liquid fuel has leaked through the filter pack and hints at the remaining fuel spray. The spray penetration pattern looks asymmetric in these images due to uneven illumination by the 284-nm laser, which is attenuated in some regions more than others; high-speed imaging of the liquid sprays indicates that all eight sprays penetrate evenly. First-stage combustion, evidenced by H_2CO-PLIF signal (red), is in progress at this crank angle and clearly visible at the head of the jet, which at this point is just impinging on the bowl wall at the right side of the image. By the next crank angle, at 364 CAD, the liquid fuel spray is no longer visible (injection has ended), while first-stage combustion continues for the next several crank angles. At 366 CAD, the first evidence of second-stage combustion (green) appears on either side of the jet centerline near the bowl wall. Second-stage ignition, as marked by the zero-crossing in the AHRR (Figure 4), occurs at approximately 363 CAD, but OH is not formed in significant quantities until the peak of the heat release, at approximately 366 CAD, as seen in Figure 7. This delay in OH-PLIF signal relative to the AHRR zero-crossing is typical of second-stage combustion [15] [26]. Spatially, second-stage combustion proceeds in recirculation regions of fuel/air mixture that have rolled up at the bowl wall. The second-stage combustion region grows larger throughout the rest of the cycle, first in the recirculation regions on either side of the jet and then across the whole width of the downstream jet near the bowl wall, starting at approximately 369 CAD. Note that during this time, the H_2CO-PLIF signal persists in most of the upstream jet, extending back to the injector tip, indicating the presence of UHC in the same region.

From 370 CAD to 375 CAD, the second-stage combustion "races back" along the jet axis, a common feature of combustion at LTC conditions [27]. During this process, the extent of the second-stage combustion reaches further back towards the injector, until the mixture is too lean to support second-stage ignition. In this case, the second-stage combustion reaches back to a radius of approximately 25 mm from the injector but no farther, leaving a large region with significant H_2CO-PLIF signal, and therefore unburned fuel, in the central region of the bowl. The downstream ignition followed by partial "racing back" behavior can be explained by a bulk gradient of increasing equivalence ratio along the jet path from the injector to the bowl wall [26]. Second-stage ignition first appears near the bowl wall, where mixtures are stoichiometric or even fuel-rich, and thereby have the shortest ignition delays. As the equivalence ratio of the fuel/air mixture along the jet path becomes leaner in regions closer to the injector, the associated ignition delay time is longer. The time required to reach second-stage ignition increases as mixtures are located closer to the injector. As a result, the racing back of second-stage combustion can be explained by successive autoignition of ever leaner mixtures. Some flame propagation may also occur simultaneously, but chemical kinetic timescales are of the correct magnitude to explain the progression solely by sequential autoignition along the equivalence ratio gradient [26]. However, some mixtures are too fuel-lean to achieve second-stage ignition in the time available before rapid cylinder expansion and subsequent charge cooling in the expansion stroke, which enforces a limit on extent of the race back.

Through the rest of the cycle, the mixture in the jet diffuses. Despite this, the two regions of reaction – first-stage combustion in the central region of the bowl and second-stage combustion in the outer regions of the bowl – remain visible. Some bright PAH-LIF/soot-LII signal is visible from 376 to 381 CAD as a small amount of soot is formed near the bowl wall, as evidenced by isolated bright red pockets.

At the end of the series (383 CAD), when Figure 4 shows the majority of combustion is complete and AHRR is nearly zero, second-stage combustion remains in the outer bowl, and first-stage combustion and thus a region of unburned hydrocarbons, evidenced by the H_2CO-PLIF signal, is still present in the central bowl region. As discussed in the Introduction, a well-timed post injection can help to reduce the level of UHC in this central region by enriching this mixture and thereby "kicking" the mixture into second-stage ignition. This should allow the second-stage reaction to "race back" even farther towards the injector tip, potentially eliminating much of this UHC source. This process will be discussed in the next section.

3.2 Main- plus one post-injection results

Figure 8 shows the effects of one post injection on load and engine-out UHC. Here, the start and duration of the main-injection duration are held constant at $SOI1_C$=352 CAD and $DOI1_C$=1000 microseconds as the post-injection duration is varied from $DOI2_C$=200 to 800 microseconds in 50 microsecond increments at $SOI2_C$=363.5 CAD. The open blue circles in Figure 8 indicate the engine-out UHC emissions with a main- plus one post-injection schedule, and the filled black circles show the variation of single-injection UHC emissions with load from Figure 6.

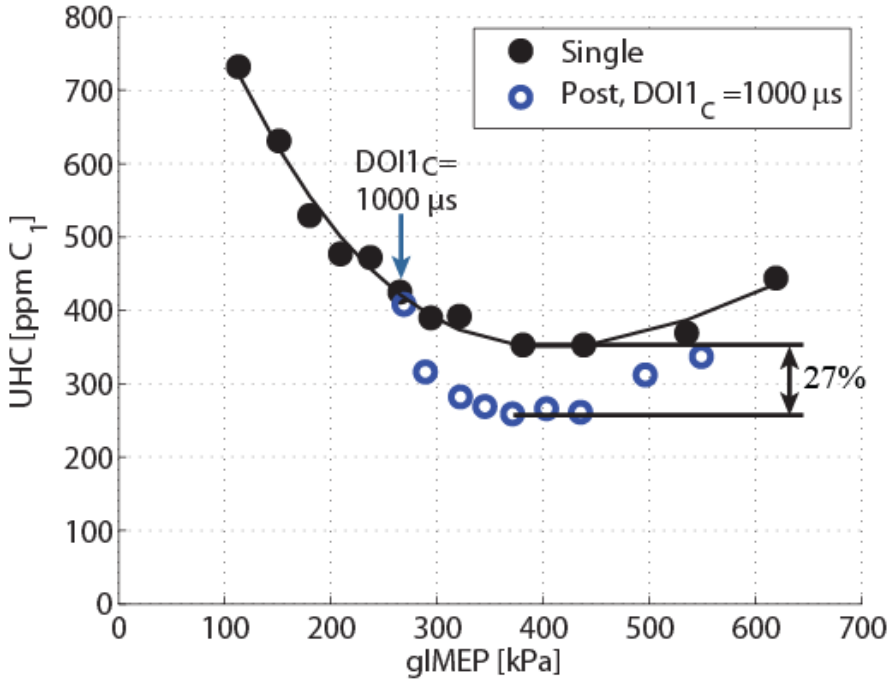

Figure 8. Engine-out UHC emissions for main- plus post-injection operation at $SOI1_C$=352 CAD, $DOI1_C$=1000 microseconds, and a range of $DOI2_C$ from 200 to 800 microseconds (open blue circles). For reference, the UHC emissions for the single-injection duration sweep of Figure 6 are also included (filled black circles and smooth fit line).

The shortest post-injection duration in Figure 8 ($DOI2_C$=200 microseconds) doesn't change engine-out UHC significantly; this is because of the very low fuel delivery of a post injection this short. Inspection of the high-speed imaging indicates that the injector is not able to reliably produce this short post injection, and so the effect of a post injection at this $DOI2_C$ is minimal.

Post injections with longer durations were much more reliable and produced significant reductions in engine-out UHC relative to single injections at comparable loads. As post-injection duration is increased initially, the engine-out UHC level decreases until $DOI2_C$=400 microseconds at 371 kPa gIMEP (approximately 100 kPa gIMEP above the main-injection only), where a minimum is reached. At this minimum, the UHC emissions are reduced by 27% compared to a single injection at the same load, as indicated on Figure 8. As $DOI2_C$ is increased further, the UHC levels increase, but are still lower than a single injection at the same load. It is evident that the main- plus post-injection schedule UHC curve seems to asymptote to the single-injection schedule curve at the longest $DOI2_C$. This may be because of the appearance of rich-source UHC as the total fuel quantity increases.

The process by which the post injection reduces engine-out UHC is shown in the LIF series in Figure 9. Mirroring the series in Figure 7 for the single injection, Figure 9 shows instantaneous images at the same crank angles.

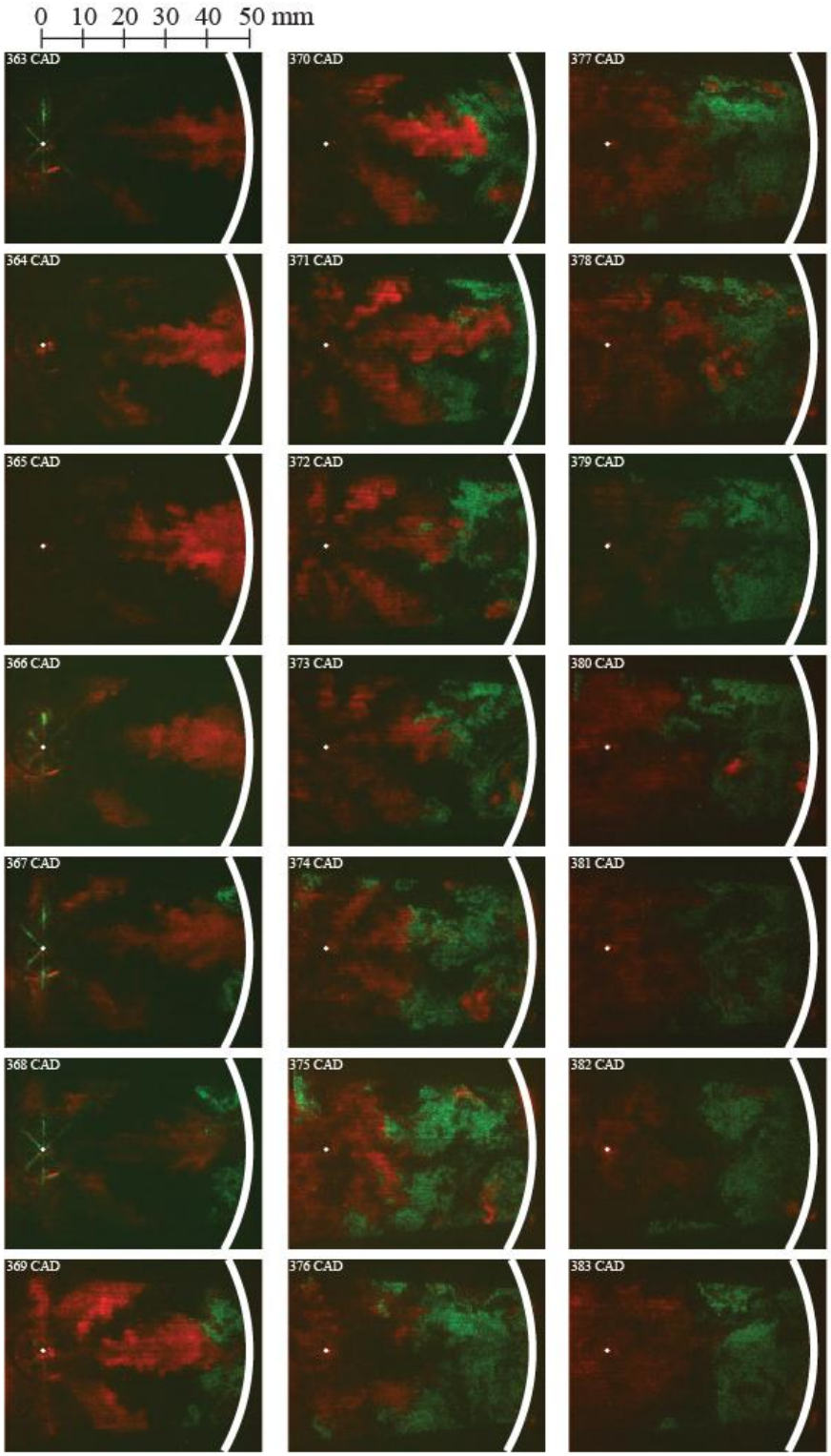

Figure 9. Simultaneous single-shot H_2CO-PLIF (false-colored red) and OH-PLIF (green) images for a main plus post-injection case at $SOI1_C$=352 CAD, $DOI1_C$=1000 microseconds, $SOI2_C$=363.5 CAD, $DOI2_C$=400 microseconds, and 371 kPa gIMEP.

The series of H_2CO-PLIF/OH-PLIF images from 363-365 CAD for the main- plus one post-injection schedule closely resemble that of the single-injection schedule in Figure 7. This is to be expected, as the main-injection combustion process is the same before the start of the post injection, which is evident at 366 CAD by the Mie scattering of the 284 nm laser off the liquid fuel of the post injection. Like before, first-stage combustion is evident in the main-injection jet as it impinges on the bowl wall and begins to spread and recirculate on either side of the jet centerline. In this series, the post injection starts near 366 CAD, only 1 CAD before any significant OH-PLIF signal from the main-injection fuel has begun. Second-stage combustion of the main-injection fuel is evident at 367 CAD, where OH-PLIF signal (green) appears in the recirculation regions on either side of the jet centerline.

The post injection ends between 368 and 369 CAD, and it leads to a greater intensity of the H_2CO-PLIF signal in the jets near the injector. Without a post injection, H_2CO-PLIF would have remained in this region because the fuel/air mixture from the main injection would have been too fuel-lean to progress into second-stage ignition (c.f. Figure 7). However, in the post-injection case, the H_2CO-PLIF signal is most likely originating from the first-stage combustion of the mixture that contains fuel from both the main and post injections. This mixture is likely more rich than a mixture without a post injection.

The results of this enriching effect can be seen from 370-377 CAD as the second-stage ignition "races back" along the jet centerline. In the post-injection case, mixtures much closer to the injector are able to achieve second-stage combustion, apparently due to the increased equivalence ratio in this region. Although the ignition delay times relative to SOI1 are still longer than those of the mixture near the bowl wall, the ignition delay for the post-injection fuel is shorter relative to SOI2, and this mixture now has enough fuel to reach second-stage combustion. OH-PLIF signal is measured as close as approximately 15 mm from the injector tip, much closer than the 25 mm that is observed in the single-injection case. This enhanced second-stage combustion near the injector provides evidence for why UHC emissions can be significantly reduced with the use of one post injection.

At later times in the cycle, from 378-383 CAD, the diffuse mixture continues to react throughout the bowl. Second-stage combustion continues in the outer bowl, while a smaller region of unburned hydrocarbons remains in the central region of the bowl. Even with one post injection, however, the second-stage ignition does not "race back" completely to the injector tip, indicating that there are still regions of unburned hydrocarbons residing in mixtures too lean to proceed to second-stage combustion. In the next section, we investigate the potential of a third injection to enrich the remaining overly-lean mixtures that were left even after the use of one post injection.

3.3 Main- plus two post-injection results

While the use of one post injection can decrease engine-out UHC, a second post injection reduces UHC levels even farther. While we did not explore a detailed parametric study with sweeps of injection timing and duration for the second post injection, Figure 10 shows the UHC levels for two different example main- plus two post-injection schedules. One of the main- plus two post-injection schedules builds on a main- plus one post-injection schedule with $SOI1_C$=352 CAD, $DOI1_C$=1000 microseconds, $SOI2_C$=363.5 CAD, and $DOI2_C$=300 microseconds (shown with a red arrow), by adding a second post injection with $SOI3_C$=367.75 CAD and $DOI3_C$=250 microseconds (red square). The other main- plus two post-injection schedule builds on a main- plus one post-injection schedule with $SOI1_C$=352 CAD, $DOI1_C$=1000 microseconds,

$SOI2_C$=363.5 CAD, and $DOI2_C$=450 microseconds (shown with a green arrow), and adds a second post injection with $SOI3_C$=370 CAD and $DOI3_C$=250 microseconds (green diamond).

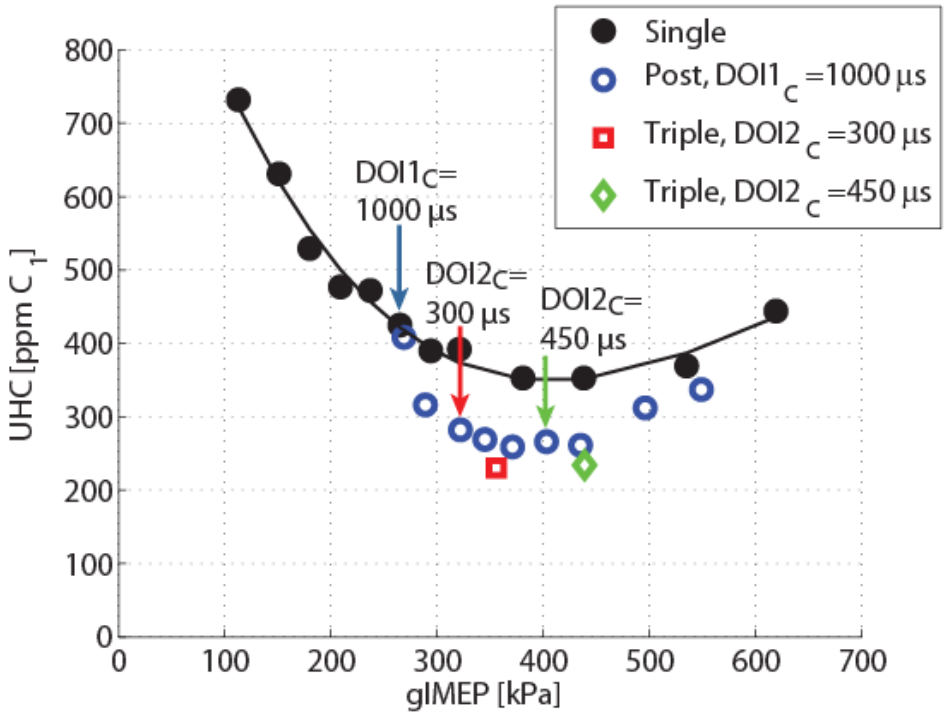

Figure 10. Engine-out UHC emissions for two different main- plus two post-injection conditions with $SOI1_C$=352 CAD, $DOI1_C$=1000 microseconds, $SOI2_C$=363.5 CAD, and either $DOI2_C$=300 microseconds, $SOI3_C$=367.75 CAD, $DOI3_C$=250 microseconds (open red square), or $DOI2_C$=450 microseconds, $SOI3_C$=370 CAD, $DOI3_C$=250 microseconds (open green diamond). The arrows show the main- plus one post-injection starting points for the two different main- plus two post-injection cases. For reference, the UHC emissions for the single-injection duration sweep of Figure 6 (filled black circles and smooth fit line) and the main plus one post-injection sweep of Figure 8 (open blue circles) are also included.

Both of these main- plus two post-injection schedules result in modest reductions of UHC emissions from the main- plus one post-injection schedule. In the case of the first post-injection duration of $DOI2_C$=300 microseconds, the second post injection reduced UHC by 36% from the single-injection schedule at the same load, or an additional 11% from the main- plus one post-injection schedule at the same load. Similarly, the main- plus two post-injection based off a first post-injection duration of $DOI2_C$=450 microseconds reduced UHC by 34% from the single-injection schedule at the same load, which is an additional 10% from the main- plus one post-injection schedule at the same load.

These non-negligible reductions in engine-out UHC achievable with a main- plus two post-injection schedule are due to the same mechanism that reduced UHC with the addition of a post injection. Figure 11 shows a series of single-shot LIF images from the $DOI2_C$=300 microseconds, $SOI3_C$=367.75 CAD, and $DOI3_C$=250 microsecond (open red square in Figure 10) main- plus two post-injection schedule at 357 kPa gIMEP.

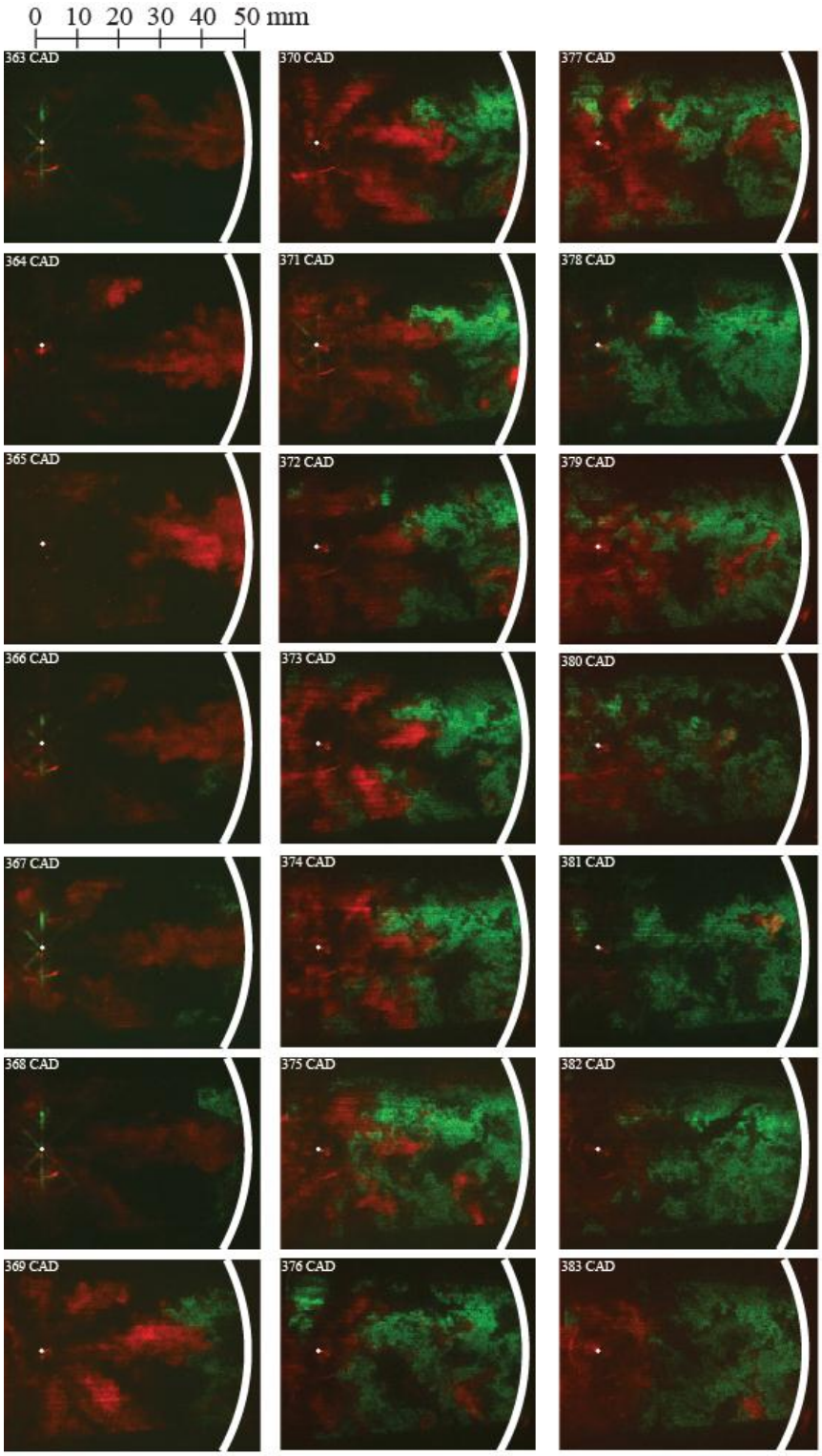

Figure 11. Simultaneous single-shot H_2CO-PLIF (false-colored red) and OH-PLIF (green) images for a main- plus two post-injection case at $SOI1_C$=352 CAD, $DOI1_C$=1000 microseconds, $SOI2_C$=363.5 CAD, $DOI2_C$=300 microseconds, $SOI3_C$=367.75 CAD, $DOI3_C$=250 microseconds, and 357 kPa gIMEP.

Once again, the series of instantaneous images in Figure 11 begins at the end of the main injection, which is evidenced by the weak Mie-scattering signal of the 284 nm laser from the liquid fuel jets (shown in green). Buildup of formaldehyde in the jet is seen for three crank angles before OH-PLIF signal appears near the bowl wall at 366 CAD. Also at this crank angle, the start of the post injection is evident the weak Mie-scattering signal. As observed in the main- plus one post-injection example in Figure 9, the second-stage combustion continues at the bowl wall while the mixture of main and post fuel and air closer to the injector remain in first-stage combustion and do not yet progress to second-stage combustion.

The "racing back" of the second-stage ignition begins at 370 CAD, evidenced by the OH-PLIF signal that begins to appear along the jet column. At 371 CAD, the liquid fuel spray of the second post-injection is barely apparent, again seen by the weak Mie scattering signal (green) in the liquid jets. This is a very short injection with a commanded injection duration of $DOI3_C$=250 microseconds, but the scattering signal shows that the actual duration is shorter, closer to 1 CAD (140 microseconds) or less. The jet from this short injection likely does not penetrate far into the bowl during the time available for combustion, and hence likely deposits fuel only in the region close to the injector.

The effect of this additional fuel addition is clear from 372 CAD to 381 CAD, where the second-stage ignition "races back" much farther than in the single-injection or the main- plus one post-injection cases. The second-stage ignition can reach farther upstream towards the injector, presumably as a result of the richer mixture created by the short third injection. Whereas in the main- plus one post-injection case where an approximately 15-mm radius zone of overly-lean mixture still existed around the injector, this is no longer the case with the second post injection, at least to 381 CAD. In several of these images, the second-stage combustion, shown by the OH-PLIF signal (green), extends all the way to the injector tip. While this would initially indicate that the second-stage combustion has accessed all of the injector-region UHC, it is important to note that these measurements are taken in one plane along the jet axis, and that the extent of the second-stage ignition throughout the depth of the combustion chamber is unknown; UHC is still measured in the exhaust, so it undoubtedly remains somewhere in the combustion chamber.

Indeed, for the later images at 382 and 383 CAD, H_2CO-PLIF signal once again begins to appear within the laser sheet in the central region of the bowl. The most likely source of this late-cycle formaldehyde (and UHC) is bulk flow motion that occurs as the piston descends during the expansion stroke. The open bowl design of this piston creates a "squish" flow during the compression stroke as fluid above the outer top surface of the piston is proportionally compressed more than fluid in the deeper bowl region. As a result, fluid is "squished" inward during the compression stroke. Likewise, during the expansion stroke, the flow is reversed, as fluid from the bowl region rushes to fill the expanding "squish" region above the outer piston top. This bulk "reverse-squish" flow can distribute fluid within the piston bowl, in this case likely drawing fluid from low in the bowl up toward the cylinder head and into the plane of the laser sheet. This fluid is below the fuel sprays during the injections, and hence cannot be accessed or enriched by the first or second post injections, at least at the injection timings explored here. As a result, even with two post injections, some H_2CO-PLIF signal, and hence UHC, remains at the end of the cycle, though the UHC levels are further reduced with the second post injection.

The optical data show that the main- plus two post-injection schedule reduces UHC emissions by the same mechanism that the main- plus post-injection schedule does: apparent

enrichment of the overly-lean region near the injector. This result opens the possibility that many other multiple-injection strategies could be designed for UHC reduction, either by altering the timing and length of the two-injection or three-injection scheme, or even adding more injections. However, additional injections will provide diminishing returns for cycle efficiency and even combustion efficiency if they are introduced later in the cycle.

4. Conclusions

In this study we have quantified the effects of multiple-injection strategies on UHC emissions at LTC conditions in heavy-duty diesel engines. Using planar laser-induced fluorescence of formaldehyde (H_2CO) and OH, we also identified the important in-cylinder fluid-mechanical and chemical-kinetic processes responsible for the engine-out UHC trends. UHC emissions at low-load conditions in heavy-duty engines are often the result of overly-lean mixtures near the injector, and can be mitigated by enriching this region using multiple injections. The major conclusions of this study are as follows:

- UHC emissions have been measured over a range of low-load, EGR-diluted, late-injection low-temperature combustion conditions in a heavy-duty optical diesel research engine. For single-injection operation, the engine-out UHC emissions are very high (>600 ppm) at the shortest injection durations tested due to occasional partial burns . UHC levels decrease as injection duration increases until a minimum is reached at an injection duration near 1400 microseconds (400 kPa gIMEP). At these mid-range injection durations, a major source of UHC is from the overly-lean region at the center of the bowl, which is created at the end of the injection. The laser-based fluorescence imaging diagnostics show that this lean region does not progress from first-stage to second-stage combustion, thereby leaving significant unburned hydrocarbons in the cylinder. Longer injections result in higher engine-out UHC levels, as a result of both lean-source UHC as well as likely incomplete combustion in fuel-rich regions.

- The addition of one post injection reduces UHC emissions over a range of post-injection durations. A minimum engine-out UHC level is achieved with a post-injection duration of 400 microseconds (increasing gIMEP by about 100 kPa), resulting in a 27% reduction in UHC emissions as compared to a single injection at the same load. Imaging of first- and second-stage combustion using H_2CO-PLIF and OH-PLIF, respectively, indicates that the post injection promotes more complete combustion in the central bowl region, likely by helping to enrich the fuel/air mixture.

- The addition of a second post injection reduces engine-out UHC by approximately 10% more, essentially by the same mechanism that is observed with the addition of one post injection. The very short second post injection does not penetrate far into the bowl, thereby promoting more complete combustion in the overly-lean area very close to the injector tip. PLIF imaging indicates that second-stage reactions occur all the way up to the injector tip with the addition of a third injection.

The results of this work provide UHC emission trends for several fuel injection parameter variations, as well as evidence for a mechanism by which UHC emissions can be reduced at LTC

conditions for heavy-duty diesel engines. Multiple-injection schedules are achievable with a wide range of injector technologies and can be implemented in existing and future diesel technologies without major engine-design changes. These results help to form a design-level understanding of multiple injections for emissions reductions at LTC conditions. Future investigations will explore the sensitivity of the post-injection efficacy to post-injection timing ($SOI2_C$) and load. A better understanding of the operational space of multiple-injection strategies should allow for more effective injection schedule design in future engine technologies.

Acknowledgements

The optical engine experiments were performed at the Combustion Research Facility, Sandia National Laboratories, Livermore, CA. Support for this research was provided by the U.S. department of Energy, Office of Vehicle Technologies. Sandia is a multi-program laboratory operated by Sandia Corporation, a Lockheed Martin Company for the United States Department of Energy's National Nuclear Security Administration under contract DE-AC04-94AL85000. The authors gratefully acknowledge the contributions of Keith Penney and Dave Cicone for their assistance in maintaining the lasers and research engine used in this study, and Dipankar Sahoo for assistance with the UHC analyzer.

References

1. Singh, S., M.P.B. Musculus, and R.D. Reitz, *Mixing and flame structures inferred from OH-PLIF for conventional and low-temperature diesel engine combustion.* Combust. Flame, 2009. **156**(10): p. 1898-1908.
2. de Ojeda, W., P. Zoldak, R. Espinosa, and R. Kumar, *Development of a fuel injection strategy for diesel LTC*, SAE International, 2008.
3. Murata, Y., J. Kusaka, M. Odaka, Y. Daisho, D. Kawano, H. Suzuki, H. Ishii, and Y. Goto, *Achievement of medium engine speed and load premixed diesel combustion with variable valve timing*, SAE International, 2006.
4. Kimura, S., O. Aoki, Y. Kitahara, and E. Aiyoshizawa, *Ultra-clean combustion technology combining a low-temperature and premixed combustion concept for meeting future emission standards.* SAE Trans., 2001. **110**(4): p. 239-248.
5. *United States Federal Register.* 2011. **76**(179).
6. *Regulation (EC) No 595/2009 of 18 June 2009*, 2009.
7. Johnson, T.V., *Review of diesel emissions and control.* Int. J. Eng. Res., 2009. **10**(5): p. 275-285.
8. Ladommatos, N., S. Abdelhalim, and H. Zhao, *The effects of exhaust gas recirculation on diesel combustion and emissions.* Int. J. Eng. Res., 2000. **1**(1): p. 107-126.
9. Plee, S.L., T. Ahmad, and J.P. Myers, *Flame temperature correlation for the effects of exhaust gas recirculation on diesel particulate and NOx emissions.* SAE Trans., 1981. **90**(4): p. 3738-3754.
10. Keeler, B. and P.J. Shayler, *Constraints on fuel injection and EGR strategies for diesel PCCI-type combustion*, SAE International, 2008.

11. Lewander, M., K. Ekholm, B. Johansson, P. Tunestål, N. Milovanovic, N. Keeler, T. Harcombe, and P. Bergstrand, *Investigation of the combustion characteristics with focus on partially premixed combustion in a heavy duty engine.* SAE Int. J. Fuels Lubr., 2008. **1**(1): p. 1063-1074.
12. Kanda, T., T. Hakozaki, T. Uchimoto, J. Hatano, N. Kitayama, and H. Sono, *PCCI operation with fuel injection timing set close to TDC*, SAE International, 2006.
13. Miles, P., D. Choi, L. Pickett, I. Singh, N. Henein, B. RempelEwert, H. Yun, and R. Reitz. *Rate-limiting processes in late-injection, low-temperature diesel combustion regimes*. in *Thermo- and Fluid-Dynamic Processes in Diesel Engines: THIESEL 2004*. 2004. Valencia, Spain.
14. Heywood, J.B., *Internal combustion engine fundamentals*1988, New York NY: McGraw-Hill, Inc.
15. Dec, J.E., *A conceptual model of DI diesel combustion based on laser-sheet imaging.* SAE Trans., 1997. **106**(3): p. 1319-1348.
16. Kim, D., I. Ekoto, W.F. Colban, and P.C. Miles, *In-cylinder CO and UHC imaging in a light-duty diesel engine during PPCI low-temperature combustion.* SAE Int. J. Fuels Lubr., 2008. **1**(1): p. 933-956.
17. Han, M., D.N. Assanis, and S.V. Bohac, *Sources of hydrocarbon emissions from low-temperature premixed compression ignition combustion from a common rail direct injection diesel engine.* Combust. Sci. Technol., 2009. **181**(3): p. 496-517.
18. Musculus, M.P.B., T. Lachaux, L.M. Pickett, and C.A. Idicheria, *End-of-injection over-mixing and unburned hydrocarbon emissions in low-temperature-combustion diesel engines.* SAE Trans., 2007. **116**(3): p. 515-541.
19. Musculus, M.P.B. and K. Kattke, *Entrainment waves in diesel jets.* SAE Int. J. Engines, 2009. **2**(1): p. 1170-1193.
20. Chartier, C., Ö. Andersson, B. Johansson, M. Musculus, and M. Bobba, *Effects of post-injection strategies on near-injector over-lean mixtures and unburned hydrocarbon emission in a heavy-duty optical diesel engine.* SAE Int. J. Engines, 2011. **4**(1): p. 1978-1992.
21. Koci, C.P., Y. Ra, R. Krieger, M. Andrie, D.E. Foster, R.M. Siewert, and R.P. Durrett, *Multiple-event fuel injection investigations in a highly-dilute diesel low temperature combustion regime.* SAE Int. J. Engines, 2009. **2**(1): p. 837-857.
22. Kashdan, J.T., P. Anselmi, and B. Walter, *Advanced injection strategies for controlling low-temperature diesel combustion and emissions.* SAE Int. J. Engines, 2009. **2**(1): p. 1835-1856.
23. Espey, C. and J.E. Dec, *Diesel engine combustion studies in a newly designed optical-access engine using high-speed visualization and 2-D laser imaging.* SAE Trans., 1993. **99**(4): p. 703-723.
24. Lachaux, T. and M.P.B. Musculus, *In-cylinder unburned hydrocarbon visualization during low-temperature compression-ignition engine combustion using formaldehyde PLIF*. Proc. Combust. Inst., 2007. **31**(2): p. 2921-2929.
25. Genzale, C.L., R.D. Reitz, and M.P.B. Musculus, *Effects of piston bowl geometry on mixture development and late-injection low-temperature combustion in a heavy-duty diesel engine.* SAE Int. J. Eng., 2008. **1**(1): p. 913-937.

26. Musculus, M.P.B., P.C. Miles, and L.M. Pickett, *Conceptual models for partially premixed low-temperature diesel combustion.* Prog. Energy Combust. Sci., 2013. **39**(2-3): p. 246-283.
27. Bobba, M.K., C.L. Genzale, and M.P.B. Musculus, *Effect of ignition delay on in-cylinder soot characteristics of a heavy duty diesel engine operating at low temperature conditions.* SAE Int. J. Engines, 2009. **2**(1): p. 911-924.